JOURNAL OF MATERIALS SCIENCE 25 (1990) 311–320

# Crystal morphology in pristine and doped films of poly (*p*-phenylene vinylene)

MICHAEL A. MASSE, DAVID C. MARTIN, EDWIN L. THOMAS, FRANK E. KARASZ
*Department of Polymer Science and Engineering, University of Massachusetts, Amherst, Massachusetts 01003, USA*

JURGEN H. PETERMANN
*Technical University of Hamburg-Harburg, Harburger Schloßstraße 20, D-2100 Hamburg 90, West Germany*

The crystal morphology of oriented films of poly(*p*-phenylene vinylene) (PPV) has been investigated using electron microscopy and X-ray diffraction. An X-ray diffraction rotation series confirmed the existence of fibre symmetry in bulk oriented films. Dark-field imaging by transmission electron microscopy (TEM) revealed small diffracting regions of the order of 7 nm in size with an aspect ratio near 1. These diffracting regions were shown by high resolution transmission electron microscopy (HREM) to be composed of small crystallites with an average size of 5 nm. Imaging of the lateral packing by HREM allowed the evaluation of local variations in crystallite orientation. This HREM method of orientation function determination compares well to bulk methods (e.g. wide-angle X-ray scattering, infrared dichroism) for PPV of similar draw ratio. A micellar model is presented to describe the crystalline morphology of oriented PPV. The model presents PPV as a highly connected network of small crystallites. The well-formed crystalline regions are thought to compose approximately 50% of the sample volume with the remainder of the volume being grain boundaries. Doping by $AsF_5$ led to the formation of an electron-dense overlayer, thought to be arsenic oxide, which prohibited dark-field imaging of the crystallites. After doping with $H_2SO_4$, crystallites of the electrically conductive phase were observed. The general morphological character is preserved in the conversion from insulating to conducting forms. For the conditions employed, the doped diffracting regions were 4 nm in size and retained the orientation initially present in the pristine film.

## 1. Introduction

Recent investigations have shown poly(*p*-phenylene vinylene) (PPV) to possess remarkable electrical and mechanical properties. Electrical conductivities of the order of $10^3(\Omega\,\mathrm{cm})^{-1}$ have been measured with bulk films treated with a variety of doping agents [1, 2]. Also, the mechanical properties of PPV are characteristic of high-modulus fibres [3]. High molecular weight PPV is conveniently synthesized through a processible precursor polymer. The highly rigid backbone renders it insoluble and infusible [4]. However, PPV precursor polymers currently under investigation are water soluble and can be cast as films [5]. The conversion to PPV is achieved by a thermally induced chemical elimination reaction. This chemical conversion is accompanied by a striking physical change. As the elimination reaction proceeds the initially flexible chain takes on the rigid character of the conjugated PPV backbone and crystallizes [6]. Furthermore, when the conversion is performed under tensile stress, a high degree of molecular orientation results [1, 6].

Previous structural studies of PPV have focused on bulk characterization of the molecular chain orientation and the crystalline structure of the pristine insulating form. Bradley *et al* [7] employed infrared dichroism to evaluate the degree of molecular orientation in drawn PPV films. This study found films drawn to $L/L_0 = 5$ to possess a Hermans orientation function of $f = 0.94$. A study by Gagnon [8] characterized the development of orientation using both infrared dichroism and X-ray diffraction. At low elongations the orientation function increased rapidly with increasing draw ratio. As the draw ratio was increased beyond 5, the X-ray derived orientation function asymptotically approached 0.96. The X-ray determined value was slightly higher than the infrared value at all draw ratios, possibly indicating a better alignment of the crystalline regions.

The crystalline structure of pristine PPV was investigated by Granier *et al.* [9] using electron diffraction. This study showed PPV to possess a monoclinic unit cell with $a = 0.790$ nm, $b = 0.605$ nm, $c = 0.658$ nm, $\alpha = 123°$, and $Z = 2$. Recent work by Granier *et al.* [10] provides a detailed description of the paracrystalline disorder inherent to PPV. No study, however, has yet been reported on the crystalline morphology of PPV.

The study of the morphological character of PPV is

0022–2461/90 $03.00 + .12 

of importance because of the complex physical transformation which occurs from the amorphous precursor to rigid crystalline PPV. The details of the physical structure will also be important in understanding the mechanical properties of PPV films. In addition, previous work in our laboratory has shown that the electrically conductive phases arising upon doping with $AsF_5$, $SbF_5$, $ClO_4^-$, and $H_2SO_4$ are crystalline [11]. However, information concerning the size and nature of the conductive crystals is lacking. This information will be crucial in the understanding of the development of the doped phase and of charge transport within bulk films.

The present study has investigated the crystalline morphology of pristine and doped PPV films. We present results obtained from conventional transmission electron microscopy (TEM). By employing diffraction contrast imaging techniques the crystallites composing the PPV films are observed. Further, high-resolution transmission electron (HREM) microscopy has been used to directly image the molecular packing within the crystallites.

## 2. Experimental procedures

### 2.1. Samples preparation

The PPV precursor polymer, poly(*p*-xylylene tetrahydrothiophenium chloride), was synthesized as previously described [5]. Films were cast from aqueous solution. Oriented polymer was obtained by stretching the films at 100 to 120° C in a heated zone apparatus. Final conversion to the fully conjugated form was conducted at 300 to 350° C in vacuum for 4 h. The final film thicknesses ranged from 10 to 20 $\mu$m.

For the electron microscopy studies, samples were prepared by two techniques. First, for SEM imaging and TEM dark-field studies the films were mechanically fibrillated using the tip of a sharp metal probe. The small microfibrillar bundles were gold coated for SEM. For TEM the bundles were sandwiched between two copper grids. A second technique was used to prepare thin films of the order of 10 to 20 nm thick for HREM. Thin sections were detached from the PPV film surface by placing the PPV on a 10% nitrocellulose/amyl acetate solution which was allowed to dry over a 24 h period. The bulk of the PPV film was then peeled from the nitrocellulose leaving behind thin sections embedded in the substrate. The sections of interest were then cut away and the substrate was dissolved using fresh amyl acetate. These thin sections of PPV were deposited on a holey carbon grid.

Microfibrillar PPV bundles were doped using both $AsF_5$ and $H_2SO_4$. In the case of $AsF_5$ doping the sample was contained in a glass vessel and evacuated to $10^{-4}$ mm Hg. The vessel was subsequently backfilled with $AsF_5$ vapour. The vapour pressure was 340 mm Hg and the doping time was varied. Sulphuric acid doping was performed by immersing PPV samples in 98% aqueous acid for 4 h. The films were then quickly rinsed in dry acetonitrile and dried under vacuum. Prior to characterization all films were handled in an argon-filled dry box. The doped TEM samples were loaded on to the microscope sample stage in the dry box. The doped samples were exposed to air for less than 5 sec while being transferred to the microscope.

Stacked bulk films totalling 100 $\mu$m thick were used for X-ray diffraction.

### 2.1. Characterization procedures

Wide-angle X-ray diffraction patterns were collected using a two-dimensional proportional counter (Siemens/Nicolet) with monochromatic Cu$K_\alpha$ radiation. The sample was mounted on a two-circle camera (Huber) allowing precise positioning.

A Jeol 35 CF scanning electron microscope was used to obtain SEM images of fibrillated PPV. The microscope was operated at 20 kV and secondary electron images were collected on Polaroid 55 P/N film.

Dark-field transmission electron micrographs were taken on a Jeol 100 CX operated at 100 kV. Dark-field images were formed using the equatorial ($g_{(1\,1\,0/2\,0\,0)}$) reflections. The diffracted beam was passed to the image plane through a 20 $\mu$m objective aperture limiting the diffracted beam to a full angular breadth of 4 mrad. Unless otherwise noted, the objective aperture was centred on the optic axis when forming the dark-field images. A total end-point dose of 0.13 C cm$^{-2}$ was measured for $g_{(1\,1\,0)}$ of PPV with 100 kV electrons. The typical imaging dose was less than 0.01 C cm$^{-2}$. This ensured that multiple exposures of the same sample region could be taken without significant beam damage. Images were collected on Kodak SO-163 electron microscope film. The latent images were developed using full strength Kodak D-19 developer with a 10 min immersion.

HREM images were taken on a Jeol 2000 FX operated at 200 kV using a tungsten filament with no objective aperture. The approximate Scherzer defocus was used with a magnification of × 130 000. Images were collected on Kodak SO-163 film and the films were processed in regular strength Kodak D-19 developer for 4 min. Optical diffraction patterns were taken from the negatives using a He–Ne laser. The spacings in the optical diffraction patterns were calibrated by comparison to a graphite standard.

## 3. Results and discussion

### 3.1. Pristine PPV

#### *3.1.1. Bulk observations*

Oriented films of PPV show anisotropy of both mechanical [3] and electrical [12] properties. The tensile strength of PPV films drawn to $L/L_0 = 5$ is 420 MPa in the direction of the molecular chain and 32 MPa in the transverse direction [3]. This mechanical anisotropy leads to an inherent tendency for oriented films to fibrillate parallel to the draw direction. Fig. 1 shows scanning electron micrographs of a section of fibrillated PPV. The draw direction is along the microfibrillar axis. In this micrograph it is evident that fibrillation along the draw direction and hence along the molecular direction prevails. The surface from which the microfibrils have been detached appears regular with long furrows at least 1 mm in length running along the chain direction. The microfibrils characteristically possess a ribbon-like morphology as can be seen from the twisted sections.

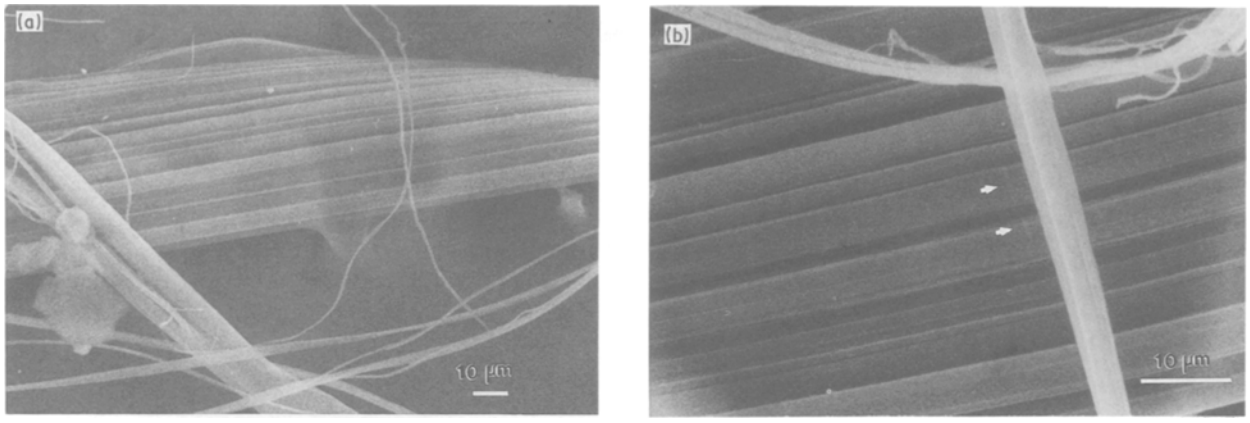


*Figure 1* Scanning electron micrographs of mechanically fibrillated PPV: (a) large PPV section showing ribbon-like morphology, (b) section showing regularity of furrows formed during mechanical detachment. Stepped regions on the microfibril surface are indicated by arrows.

To investigate the existence of a preferred planar orientation X-ray diffraction patterns were collected from bulk films. Fig. 2 shows the scattered equatorial intensity along the equator of the diffraction pattern for three rotation angles. The oriented films have been rotated about the draw direction by an angle $\beta$. The incident beam is normal to the film surface $\beta = 0°$. Along the equator the (1 1 0), (2 1 0), and (3 1 0) reflections are seen at all rotation angles. Further, no change in relative intensities observed as the oriented film is rotated. Thus, from a macroscopic point of view the films possess fibre symmetry. Also, electron diffraction patterns of thin sections always show the presence of more than one family of lateral crystallographic spacings (i.e. (1 1 0), (2 1 0), (3 1 0), etc.) indicating that fibre symmetry extends to very local regions of the film. Because preferred orientation within the plane of the film is absent, the observed fibrillation behaviour is thought to result primarily from the high degree of molecular orientation in the draw direction.

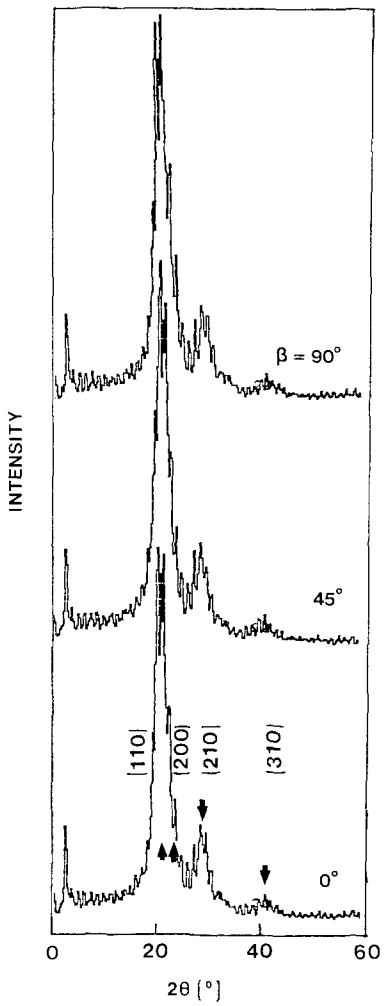


*Figure 2* Equatorial diffracted X-ray intensity for different rotation angles. Here the films are rotated about the draw direction. The angle between the incident X-ray beam and the film normal is indicated.

### 3.1.2. Crystal morphology

A $g_{(1\,1\,0/2\,1\,0)}$ dark-field transmission electron micrograph of oriented PPV ($L/L_0 = 8$) is shown in Fig. 3. The average dimension of the crystallites was determined by measuring 40 to 50 crystallites in a given micrograph. The average size of the diffracting

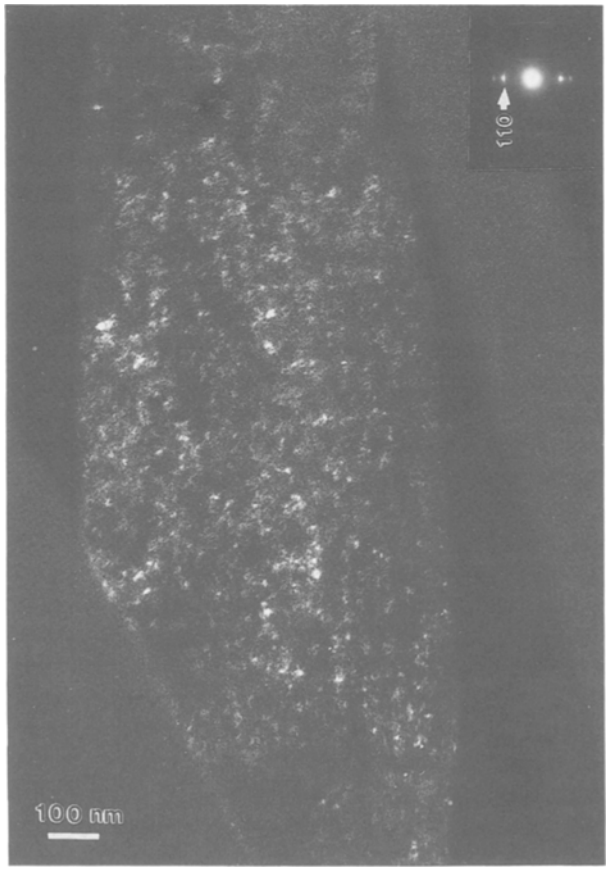


*Figure 3* Dark-field image ($g_{(1\,1\,0/2\,0\,0)}$) of oriented PPV. The draw ratio ($L/L_0$) is 8 and the molecular axis is vertical.

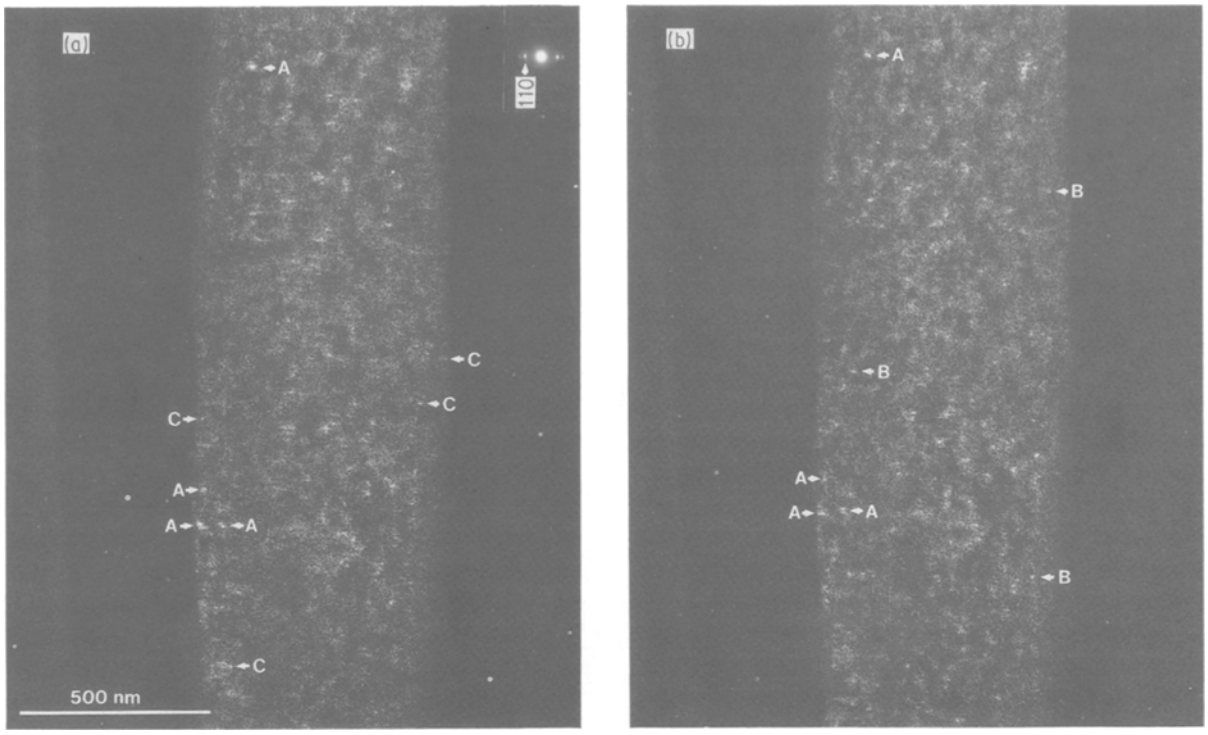


*Figure 4* Displaced aperture tilt series of dark-field ($g_{(110/200)}$) images. The draw ratio of the film is 8. The incident beam is normal to the sample surface for (a) and tilted by 0.26° in (b). A, Crystallites which are undergoing a change in diffracting intensity but are observed at both orientations; B, crystallites disappearing after tilt; C, crystallites appearing after tilt.

regions shown in Fig. 3 is 6.9 nm with a standard deviation of 3.1 nm. As observed here, the aspect ratio of the crystallites is near 1.0. This image gives the impression that only short crystallites exist. Ordered fibres of other rigid rod polymers such as poly(*p*-phenylene benzobisthiazole) (PBZT) and poly(*p*-phenylene benzobisoxazole) (PBZO) also possess short crystallites of the order of 5 to 10 nm [13, 14].

Although the diffracting regions appear equiaxed, a single dark-field image does not preclude the possibility of a structure involving long needle-like crystals with a tendency to twist about the crystallite axis. If the latter is the case, then while a small section of the crystallite is meeting the Bragg condition and diffracting, neighbouring segments along the crystallite would be twisted out of the Bragg condition and appear dark. To investigate whether this occurred in PPV, dark-field images were taken before and after tilting the incident electron beam. This technique has been previously discussed by White and Thomas [15] and allows precise determination of tilt angles as small as 0.1°. If the crystals were needle-like in morphology, then after tilting, their diffracting intensity would translate along the draw direction as new segments of the twisted crystal came into the Bragg condition. Fig. 4 shows a dark-field image of PPV before and after a beam tilt of 0.26° about the chain axis. A relatively small tilt angle was chosen so that the majority of initially diffracting crystals would also be present in the second image. In this way the crystallite locations are more easily correlated between the two images. While all crystallites are observed to undergo a change in diffracting intensity upon beam tilting only a small fraction of the total population comes into or goes out of the Bragg condition. Those regions labelled A in Fig. 4 are observed both before and after tilting. However, crystallites labelled B appear after the tilt and those labelled C disappear. This is expected for small beam tilts and is illustrated in the $g_{(110)}$ rocking curve (Fig. 5) where the orientations of crystallites A, B and C are shown before and after tilting. In no case did the intensity of a single diffracting region translate along the draw direction as the beam was tilted. This result shows that a needle-like crystal morphology can be ruled out. Thus the rigid character of the polymer chain does not manifest itself by forming extended crystals along the chain axis. Rather the diffracting regions are equiaxed, with an average length of 7 nm.

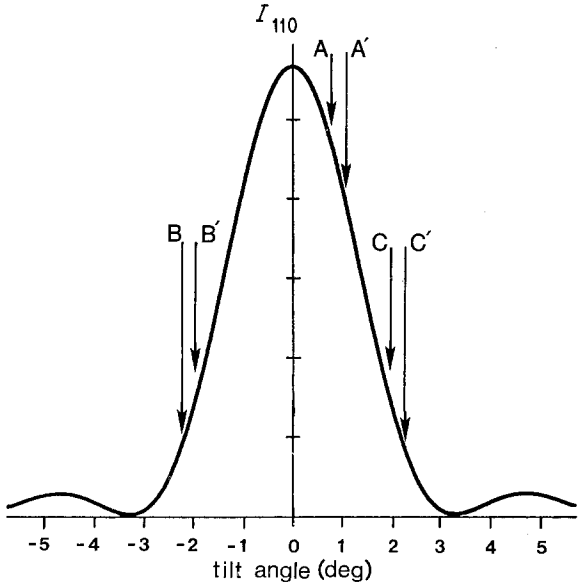


*Figure 5* Rocking curve for $g_{(110)}$ of PPV. A crystal thickness of 7.5 nm was used in the calculation. A, B, and C correspond to the crystallites indicated in Fig. 5. The primed letters show the intensity after a beam tilt of 0.26°.

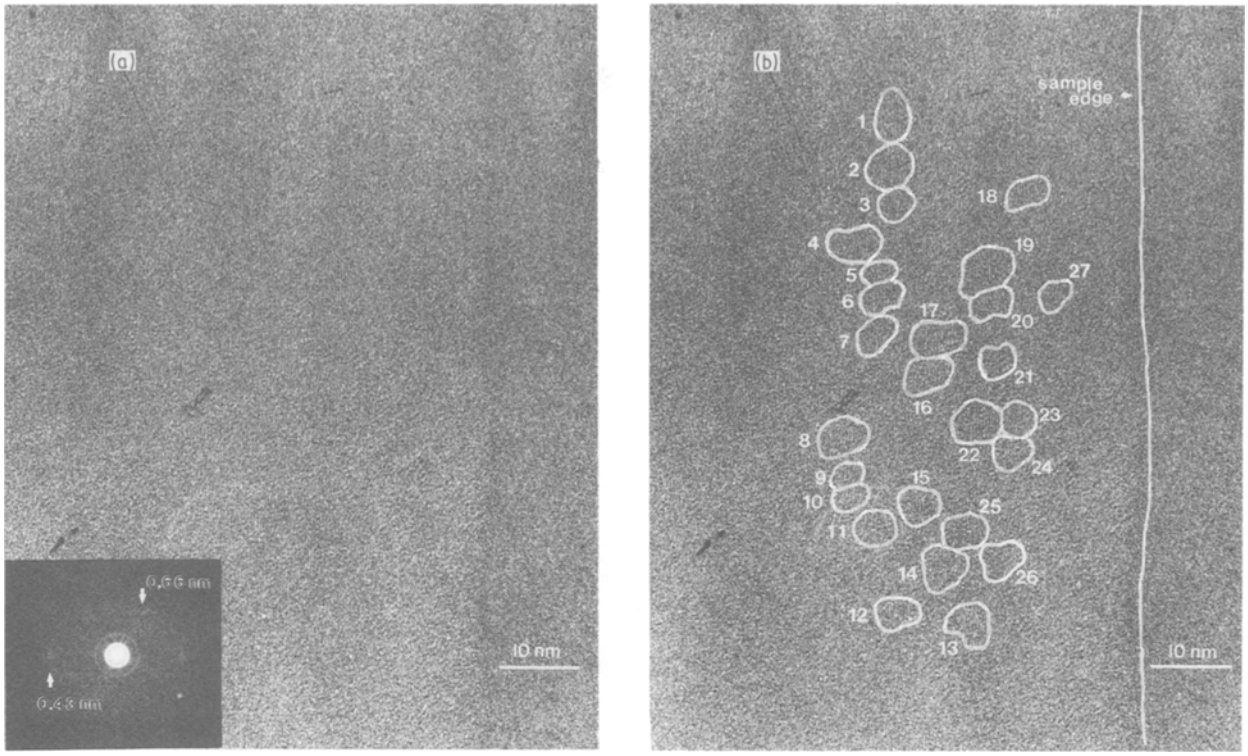


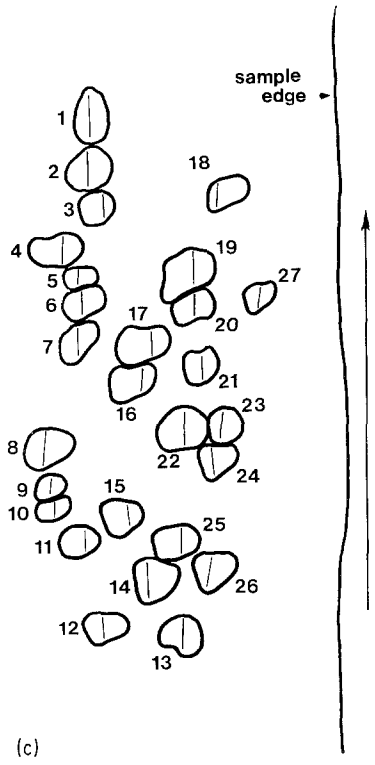


*Figure 6* High-resolution transmission electron micrograph of PPV (draw ratio = 9.3). (a) Micrograph showing 0.43 nm lattice fringes. The inset shows the optical diffractogram from this image. (b) The same micrograph but with the individual crystallites outlined. (c) Schematic representation of the crystallite orientations.

A high-resolution image of a thin PPV section ($L/L_0$ = 9.3) is shown in Fig. 6. Close inspection of Fig. 6a shows lattice fringes running parallel to the film edge. From the optical diffraction pattern the spacing of the fringes is measured as 0.43 nm. This corresponds to the (1 1 0) crystallographic spacing in the PPV crystal. Hence, this micrograph allows direct observation of the molecular packing in the oriented crystals. The optical diffraction pattern also shows a weaker periodicity corresponding to the (0 0 1) reflection. Because of the monoclinic symmetry of the PPV unit cell this reflection appears off the meridian. The (0 0 1) fringes ($d$ = 0.658 nm) while present are not obvious in the micrograph itself.

In Fig. 6b the individual crystallites are outlined. The criterion for identification of an individual crystallite is that the fringes must be continuous both laterally and axially. Further, the fringes within one crystallite must have the same orientation. Thus, relatively large regions displaying fringes can be divided into separate grains. This is clearly seen by comparing crystallites 23 and 24 in Fig. 6b. These neighbouring crystallites differ in orientation by 11°. The crystallites and their orientations are shown schematically in Fig. 6c. As can be seen they are highly aligned in a film with a draw ratio of 9.3. In Fig. 7 a histogram representing the crystallite orientations is shown. Here the crystallite orientations have been measured with respect to the film edge. The average orientation angle is $-1°$ (clockwise being positive) but the individual orientations range from $-9°$ to $+6°$. Using the orientation angles, $\phi$, shown in Fig. 7 for the 27 crystals observed, $\langle\cos^2\phi\rangle$ can be calculated directly; the Hermans orientation function is 0.94. This is very close to the value of $f$ = 0.95 measured by X-ray diffraction for PPV of $L/L_0$ = 8.3 [8].

It is important to note that the maximum observed crystallite misorientation from the draw direction is only 9°. A recent study by Simpson *et al.* [16] has employed $^2$H broadline nuclear magnetic resonance spectrometry (NMR) to evaluate the molecular orientation in drawn PPV films. These investigators observed an orientation distribution which was well modelled by two superposed Gaussian distributions.

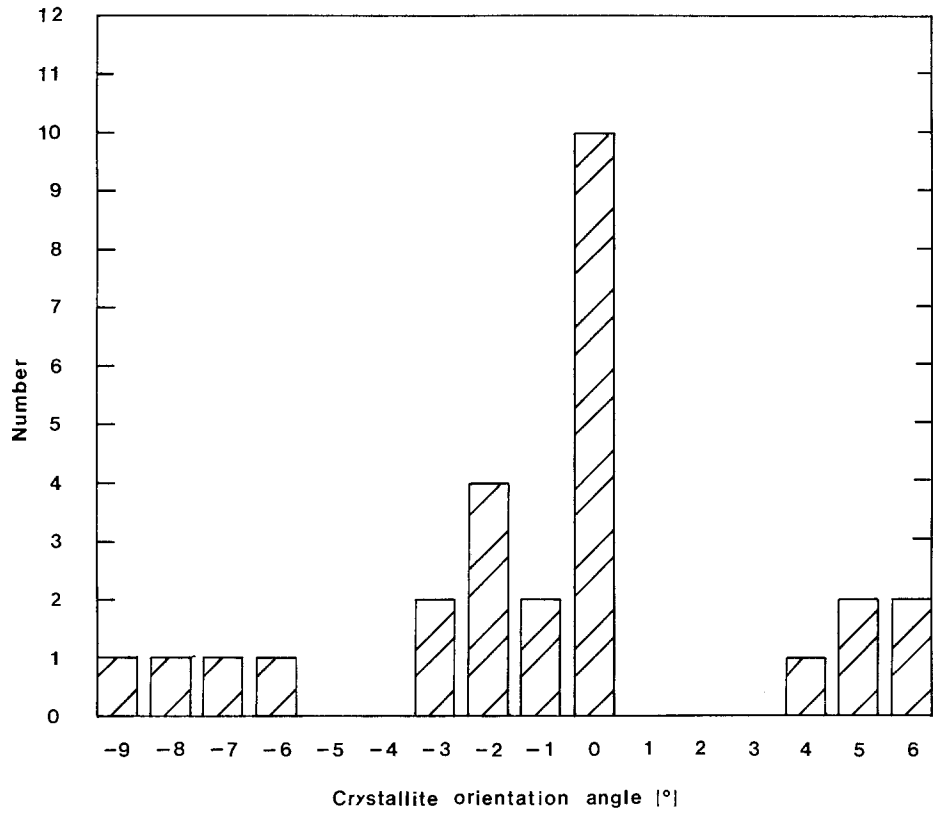


*Figure 7* Orientation distribution of the crystallites observed in the HREM image (Fig. 6).

Each of the two Gaussian profiles has an essentially equal contribution to the total and has a distribution width ($\Delta\beta$) of 9.5° and 30° respectively. NMR lineshape simulations, though, cannot unequivocally determine whether each component of the simulation corresponds to a separate fraction of the material or simply results from a complex distribution of a single fraction. Our direct HREM observations, however, suggest that the $\Delta\beta = 9.5°$ component can be associated with the well-oriented crystallites. Also, because NMR probes ordered as well as disordered molecular chains, information regarding the fraction of well-oriented crystallites can be inferred. Because in the NMR simulations the narrow distribution component constitutes 50% of the total, it is reasonable to expect approximately half of the PPV repeat units to exist in well-oriented crystallites. The remaining 50% of the repeat units might be supposed to exist in severely misoriented crystallites. Such crystallites, however, were not observed by HREM which images all diffracting (1 1 0) crystallites regardless of their *c*-axis orientation. As already stated for the crystallite population observed, an angular breadth of misorientation of only 15° was seen. It is thus more likely that the broad distribution component corresponds to PPV chains in the disordered grain-boundary regions.

From the lattice image, the individual crystallite sizes can be readily measured. On average, the crystallites in Fig. 6 are 5.6 nm long and 4.4 nm wide with both the lateral and longitudinal dimensions having standard deviations of 0.9 nm. As can be seen from Fig. 6b the individual crystallites are not isolated in all cases but may exist closely spaced in clusters. The latter range in size from 5 to 10 nm. In dark-field imaging, clusters with crystallites misoriented by up to approximately $\pm 5°$ would appear as a single diffracting region because an aperture of finite size was used. Indeed, the cluster sizes obtained from lattice images agree well with the size of the diffracting regions in the dark-field images. It is important to note that these results indicate that diffracting regions observed in the dark-field image are not necessarily individual crystallites but could correspond to clusters of neighbouring crystallites having similar but not identical orientations.

The oriented films thus contain equiaxed oriented crystals connected by regions of disordered chains. The well-ordered crystallites make up approximately 50% of the sample volume with the remaining material located in grain boundaries. Because the disordered chains in the grain boundaries cannot be directly observed by dark-field TEM their orientational state remains uncertain. However, a truly amorphous phase is not expected because of the rigid character of the PPV chain. Rather the molecular chains in the grain boundary are likely to exist in a relatively disordered state with no long-range periodicity. A high degree of connectivity between crystallites in the form of tie molecules is also required to be consistent with the good mechanical properties observed in PPV [3]. Further, preliminary neutron scattering results on isotropic polycrystalline films of PPV have indicated that a single chain traverses many crystallites [17]. Thus, oriented PPV can be thought of as a highly connected network of equiaxed crystallites. Fig. 8 shows a schematic illustration of this micellar morphology.

### 3.1.3. Kink band morphology

Another feature which is apparent in the dark-field images is the presence of dark bands within the

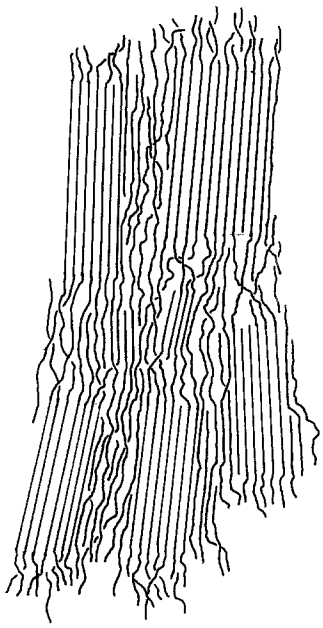

*Figure 8* Schematic representation of the micellar crystal morphology of PPV. The crystallites are approximately 5.0 nm wide and long.

diffracting film (Fig. 9). Typically these bands extend from the film edge nearly perpendicular to the draw direction. To determine whether these regions were non-crystalline, a tilt-rotate series was conducted. Neither tilting of the film about the fibre axis nor tilting about the axis lying in the plane of the film and perpendicular to the fibre axis changed the appearance of the dark-field image. However, a rotation of the sample about a vector normal to the surface or an azimuthal displacement of the objective aperture (see Fig. 9d) caused illumination of these regions. Fig. 9 shows the images resulting from successive displacements of the objective aperture. While Figs 9b and c are displaced aperture dark-field images, the displacement is small (Fig. 9d), and the effect of aberrations on image quality is minimal. Fig. 9a shows a dark-field image of a sample having dark bands. This image was formed with the objective aperture centred on the (2 0 0/1 1 0) combined reflection. At this sample orientation, the bands are only slightly darkened. Fig. 9b shows the dark-field image resulting after a $-20°$ azimuthal displacement of the objective aperture. Here, the crystallites of the band are illuminated while the rest of the film is dark. In this position the aperture permits the passage of $\boldsymbol{g}_{(1\,1\,0/2\,0\,0)}$ beams diffracted from crystals misoriented by $-20°$ from the fibre axis. For an azimuthal displacement of $+20°$ the contrast of film and band is reversed, as shown in Fig. 9c.

This series indicates that the bands are crystalline but are characteristic of an orientational defect. Further, the defect can be identified as a rotation of approximately 20° about the film normal. This orientational defect is schematically represented in Fig. 10. As shown in this figure the orientational disorder is represented as purely lateral. This is not meant to exclude the possibility of a component of the displacement normal to the film surface. In fact, there are features apparent from SEM (Fig. 1b) which suggest the presence of stepped regions on the surface of the PPV microfibrils. These regions, like the bands observed in dark-field imaging, extend from the film edge perpendicular to the draw direction. Thus while the band deformation appears to have a large lateral component some evidence exists for the presence of a component normal to the film surface.

Kink bands have been observed in other high-modulus fibres [18–20] and are characteristic of a microbuckling response to axial compressive forces. The character of the dark bands observed in PPV suggests that these, too, are kink bands. As such, these bands may not be present in bulk films of PPV but may result from the mechanical action of sample preparation. The effect of the deflection associated with a 20° misorientation should present minimal resistance to charge carrier transport. However, if cleaved or sharply kinked chains existed at these kink band boundaries, disruptions in the conjugated nature of the chain would occur and the carriers could be severely impeded leading to low electrical conductivities. Also, as observed in high-modulus fibres [21], the presence of these kink bands suggests a low compressive strength of PPV in the chain direction.

## 3.2. Doped PPV

The doped electrically conductive phases of PPV are crystalline and structurally different from the pristine crystal. We have previously determined that PPV films doped with $AsF_5$, $SbF_5$, or $H_2SO_4$ possess the same crystalline orthorhombic symmetry with only slight variations in *d*-spacings for the different complexes [11]. In the doped complexes planar polymer chains form stacks with an intermolecular separation of 0.33 nm within the stacks. The distance between stacks is of the order of 1.0 nm. These stacks are separated by a plane containing dopant anions. The conjugated character of the PPV chain leads to high electrical conductivities along the chain direction. It is noted that the transverse conductivity is only 30 to 50 times less than that in the chain direction for highly oriented films [12]. This significant transverse conductivity is accounted for by the excellent overlap of $\pi$-orbitals in the conducting crystals [11].

Dark-field images were taken of doped PPV films to examine the size and spatial distribution of these conductive crystals. Fig. 11 shows dark-field images of $AsF_5$ doped films. The PPV film shown in Fig. 11a was doped for 75 min. The electron diffraction pattern of this film indicated that the crystallites imaged with this history still represent undoped PPV. Circular regions of relatively high electron density appear at this low doping level and are seen as dark regions in the micrograph. These electron dense regions grow as the doping level is increased. Fig. 11b shows a film doped with $AsF_5$ for 160 min. At this point the electron diffraction pattern is very diffuse. This is thought to arise from the increased electron density of the doped film and the resulting increased inelastic scattering. As a result, no contrast corresponding to individual crystallites can be observed in the image. Further, the electron-dense regions have increased in size with the largest ones appearing spherical. This electron-dense overlayer is consistent with the

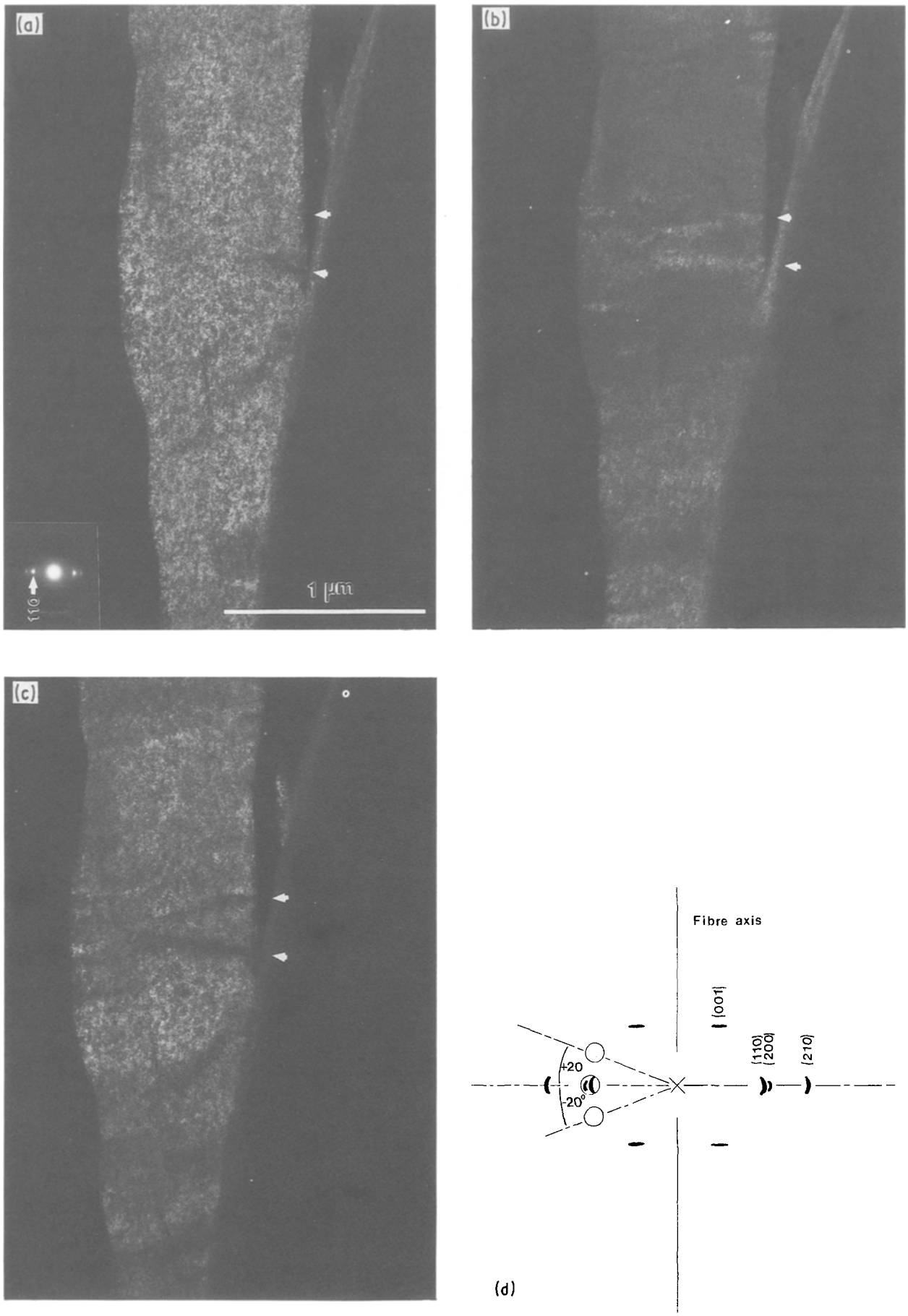


*Figure 9* Rotation series showing crystallites in misoriented bands (draw ratio = 8). (a) Dark-field image with aperture centred on $g_{(110/200)}$. (b) Image formed with aperture rotated by approximately $+20°$. (c) Image formed with aperture rotated by approximately $-20°$. (d) Schematic representation of aperture placements.

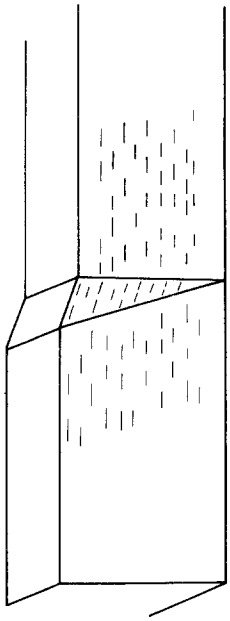

*Figure 10* Schematic representation of crystallite orientation in and around misoriented bands.

incorporation of arsenic oxide in $AsF_5$-doped PPV [11]. Because of the propensity of $AsF_5$-doped PPV to form an electron-dense layer, it was not possible to obtain dark-field images of the doped crystallites even on the thinnest sections.

Sulphuric acid-doped samples, on the other hand, were amenable to dark-field study. Fig. 12 shows a dark-field image of $H_2SO_4$-doped PPV. The electron diffraction pattern shown in the inset confirms the crystallinity and a high degree of orientation. No indication of undoped regions was apparent from the diffraction patterns. Further, no electron-dense overlayer was observed on $H_2SO_4$-doped films. The 1.04 nm equatorial spacing ($g_{(100)}$) characteristic of this complex is seen (Fig. 12) close to the main beam. The intense $g_{(200)}$ reflection at 0.52 nm was used to form these dark-field images. As in the pristine sample, $H_2SO_4$-doped PPV shows small crystallites evenly dispersed throughout the film. The contrast is, in general, lower than seen in the pristine films. On average the crystallites are 4.4 nm in size with a standard deviation of 1.4 nm. The resulting conductive crystals, while well formed, are slightly smaller in dimension than the undoped crystals. Further, the general morphological character is the same for both pristine and doped films. Thus the micellar model of the pristine films can also describe the doped morphology. However, because the doped crystallites appear significantly smaller than the pristine crystallites the sample volume composed of well-ordered doped crystallites may be less than 50%.

From the above results, conclusions can be drawn concerning the physical transformation of oriented PPV occurring during doping. As the film is converted to its electrically conductive form the pristine crystallites undergo a crystal–crystal transformation [11]. At low doping levels (Fig. 11a) only pristine crystallites are observed in thin films. However, even for doping times on the order of 10 min bulk films demonstrate high electrical conductivities [11]. Thus, at low doping levels a continuous conductive pathway must exist along the length of the film. Because pristine crystals

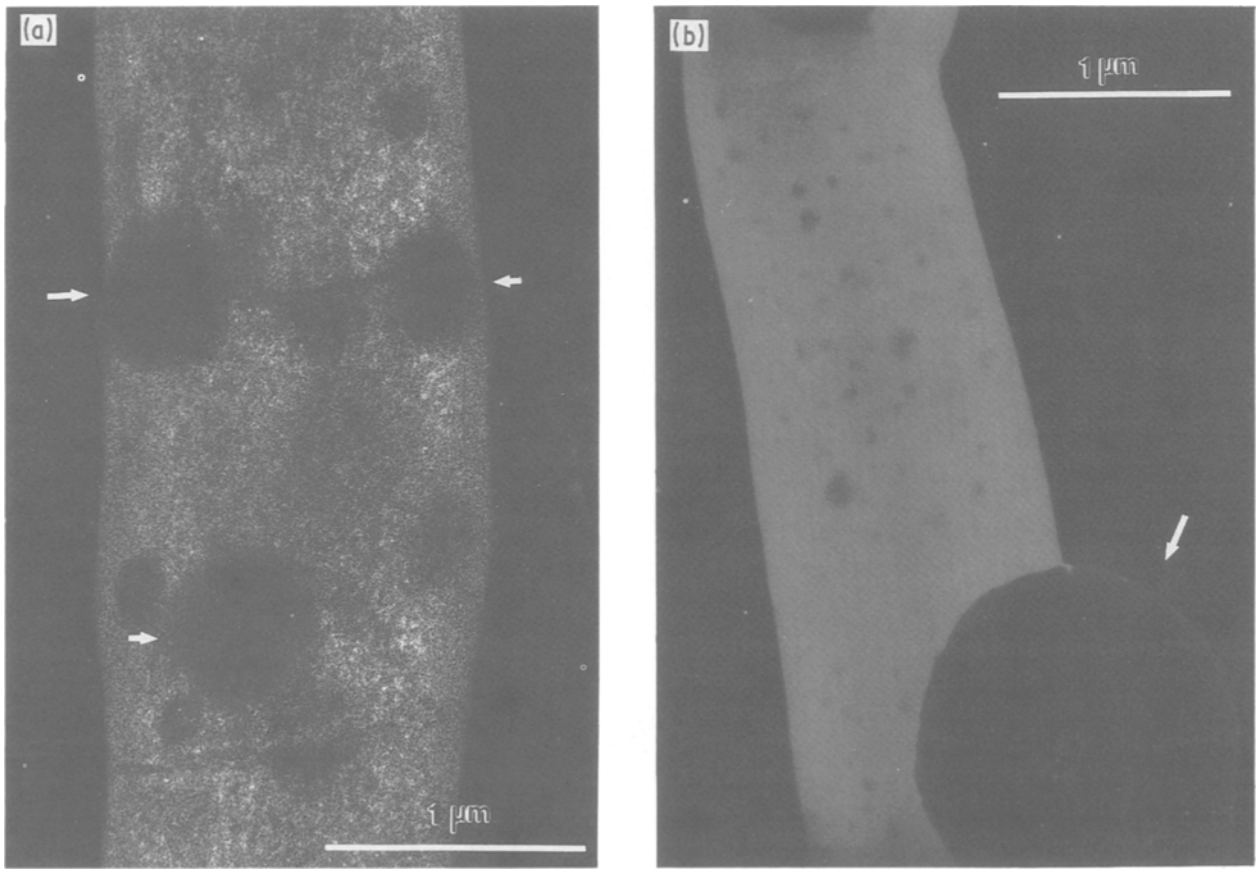


*Figure 11* Equatorial dark-field images of $AsF_5$-doped PPV (draw ratio = 8): (a) film doped for 75 min, the circular electron dense regions are indicated, (b) film doped for 160 min, the spherical electron dense regions are indicated.

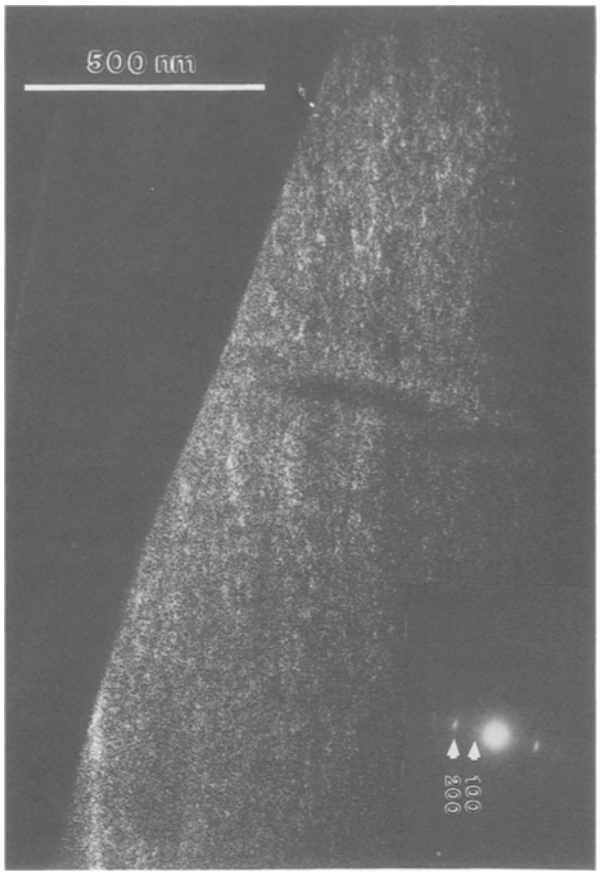


*Figure 12* Dark-field image ($g_{(200)}$) of $H_2SO_4$-doped PPV (draw ratio = 8). The inset shows the electron diffraction pattern. The (2 0 0) reflection is indicated.

appear largely intact at low doping levels it is reasonable to expect that the grain boundaries are preferentially converted to the conductive phase in the early stages of doping, leaving the bulk of the pristine crystallites unmodified. As doping proceeds the conductive phase would be expected to grow at the expense of the pristine crystallites until only the latter material exists in the fully doped condition (Fig. 12).

## 4. Conclusions

Oriented films of poly(*p*-phenylene vinylene) have been shown to possess small crystallites approximately 5.0 nm in size with aspect ratios near 1.0. A micellar model describing the crystalline morphology is presented. According to this model oriented PPV is composed of a highly connected network of well-formed crystallites making up about half of the sample volume. In this morphology a significant fraction of the polymer chains exists in disordered grain-boundary regions. While this disorder may serve as an impediment to charge carriers in the doped films it is expected to allow facile diffusion of dopants in the PPV films.

The local degree of molecular orientation has been evaluated by direct observation of the molecular packing. Using HREM, the orientation function for PPV can be calculated from a relatively small number of crystallites. In PPV the local evaluation of molecular orientation agrees well with bulk determinations.

Kink bands characteristic of mechanical failure due to compressive axial forces are also observed in thin sections of PPV. It is yet to be determined whether this type of defect arises during sample fibrillation or is present in pristine films.

As the films are doped, the general morphological character remains unchanged. At low doping levels the conductive regions are unobservable and are thought to be located in the grain-boundary region between pristine crystallites. At complete conversion, well-formed crystallites of the conductive phase formed by $H_2SO_4$ doping are observed. These crystallites, however, are somewhat smaller than the pristine crystallites.

## Acknowledgements

The authors thank Dr D.M. Rice for helpful discussions concerning NMR of oriented PPV. MAM thanks the Plastics Institute of America for a supplemental fellowship. DCM acknowledges doctoral fellowship support from the Shell Co. This work was supported by AFOSR grants 88-001 (FEK) and 85-0275 (ELT).

## References

1. F. E. KARASZ, J. D. CAPISTRAN, D. R. GAGNON and R. W. LENZ, *Molec. Cryst. Liq. Cryst.* **118** (1985) 327.
2. I. MURASE, T. OHNISHI, T. NOGUCHI, M. HIROOKA and S. MURAKAMI, *ibid.* **118** (1985) 333.
3. J. M. MACHADO, M. A. MASSE and F. E. KARASZ, *Polymer* in press.
4. K. D. GOURLEY, C. P. LILLYA, J. R. REYNOLDS and J. C. W. CHIEN, *Macromol.* **17** (1984) 1025.
5. R. W. LENZ, C. C. HAN, J. STENGER-SMITH, and F. E. KARASZ, *J. Polym. Sci. Chem.* **26** (1988) 3241.
6. D. D. C. BRADLEY, *J. Phys. D. Appl. Phys.* **20** (1987) 1389.
7. D. D. C. BRADLEY, R. H. FRIEND, H. LINDENBERGER, and S. ROTH, *Polymer* **27** (1986) 1709.
8. D. R. GAGNON, PhD dissertation, University of Massachusetts (1986).
9. T. GRANIER, E. L. THOMAS, D. R. GAGNON, F. E. KARASZ and R. W. LENZ, *J. Polym. Sci. Phys.* **24** (1986) 2793.
10. T. GRANIER, E. L. THOMAS and F. E. KARASZ, *ibid.* **27** (1989) 469.
11. M. A. MASSE, J. B. SCHLENOFF, F. E. KARASZ and E. L. THOMAS, *ibid.* in press.
12. D. R. GAGNON, J. D. CAPISTRAN, F. E. KARASZ and R. W. LENZ, *Polym. Bull.* **12** (1984) 293.
13. J. R. MINTER, K. SHIMAMURA, and E. L. THOMAS, *J. Mater. Sci.* **16** (1981) 3303.
14. S. J. KRAUSE, T. B. HADDOCK, D. L. VEZIE, P. G. LENHERT, W-F. HWANG, G. E. PRICE, T. E. HELMINIAK, J. F. O'BRIEN and W. W. ADAMS, *Polymer* **29** (1988) 1354.
15. J. R. WHITE and E. L. THOMAS, *J. Mater. Sci.* **20** (1985) 2169.
16. J. H. SIMPSON, D. M. RICE and F. E. KARASZ, *Macromol.* submitted.
17. H. MATTOUSSI and F. E. KARASZ, unpublished results, 1988.
18. S. J. DeTERESA, S. R. ALLEN, R. J. FARRIS and R. S. PORTER, *J. Mater. Sci.* **19** (1984) 57.
19. E. J. ROCHE, T. TAKAHASHI and E. L. THOMAS, *ASC Sympos. Ser.* **141** (1980) 303.
20. M. G. DOBB, D. J. JOHNSON and B. P. SAVILLE, *Polymer* **22** (1981) 960.
21. S. J. DeTERESA, R. S. PORTER and R. J. FARRIS, *J. Mater. Sci.* **23** (1988) 1886.

*Received 16 January*
*and accepted 13 February 1989*